Journal of The Electrochemical Society, **154** (6) G141-G146 (2007)
0013-4651/2007/154(6)/G141/6/$20.00 © The Electrochemical Society

Structural and Electrical Investigations of Pulse-Laser-Deposited (Pb,Sr)TiO_3 Films at Various Oxygen Partial Pressures

Jyh-Liang Wang,[a,z] Yi-Sheng Lai,[b] Sz-Chian Liou,[c] Chen-Chia Chou,[d] Chun-Chien Tsai,[a] Chun-Ping Juan,[a] Huai-Yuan Tseng,[a] Chueh-Kuei Jan,[a] and Huang-Chung Cheng[a]

[a]*Department of Electronics Engineering and Institute of Electronics, National Chiao Tung University, Hsinchu 30010, Taiwan*
[b]*Department of Materials Science and Engineering, National United University, Miaoli 36003, Taiwan*
[c]*Center for Condensed Matter Sciences, National Taiwan University, Taipei 10617, Taiwan*
[d]*Department of Mechanical Engineering, National Taiwan University of Science and Technology, Taipei 10607, Taiwan*

Pulsed-laser deposited (Pb,Sr)TiO_3 (PSrT) films on Pt/SiO_2/Si substrate deposited at various oxygen partial pressures (P_{O_2}), ranging from 50 to 200 mTorr, were investigated in this work. PSrT films exhibit (100) preferred orientation at lower P_{O_2} and then transit to (110) preferred orientation above 100 mTorr. The paraelectricity/ferroelectricity transition and dielectric constant of PSrT films are associated with the preferred orientation and oxygen concentration at various P_{O_2}. Furthermore, films deposited at higher P_{O_2} exhibit higher breakdown field and smaller leakage current density as a consequence of fewer oxygen vacancies. Except for the case of films deposited at 200 mTorr, the conduction mechanism is identified as Schottky emission/Poole–Frenkel emission at low/high electric fields.
 [DOI: 10.1149/1.2728148]

Manuscript submitted August 31, 2006; revised manuscript received February 9, 2007. Available electronically April 30, 2007.

$PbTiO_3$ (PTO) film has been considered for applications in nonvolatile random access memory (NVRAM), but many drawbacks of this film must be improved, such as high coercive field, high crystallization temperature, and poor microstructure. The (Pb,Sr)TiO_3 (PSrT) is composed of the solid solutions: $PbTiO_3$ (PTO) and the $SrTiO_3$ (STO). PTO and STO films, at room temperature, behave in a tetragonal structure (ferroelectric phase) and a cubic structure (paraelectric phase), respectively, because PTO has the Curie temperature (T_c) at 490°C and STO has the T_c at −220°C. The effects of lead substituted by strontium (Sr) in the PTO film decrease the crystallization temperature and offer good control of the dielectric properties at room temperature.[1,2] Therefore, PSrT is suitable for memory, sensor, frequency tuning devices, and microwave applications due to its large electric-field-dependent dielectric constant and composition-dependent Curie temperature.[1-6] In this work, (Pb,Sr)TiO_3 films were prepared using pulsed-laser deposition (PLD), which is simple, versatile, and capable of growing a wide variety of stoichiometric oxide films without subsequent high-temperature annealing and is excellent for fabricating ceramic films with complex compounds. Hence, PLD is a potential technique which could be integrated into low-temperature semiconductor processing to suppress the formerly deposited underlayers from damage and eliminate the volatilization of PbO in lead-titanate-based thin films, which always degrades the crystallinity of perovskite phases and electric properties of ferroelectric devices.[7]

The PLD process consists of three steps:[8] (*i*) vaporization of a target material by laser beam, (*ii*) transport and interaction of a vapor plume with a background ambient, and (*iii*) condensation of the ablated material onto a substrate where a thin film nucleates and grows. Hence, the structural and electrical characteristics of the PLD ferroelectric films are strongly affected by processing parameters such as substrate temperature, laser energy fluence (laser power density), and oxygen ambience.

To our knowledge, much less is known about the ambient oxygen effect on PLD ferroelectric films,[9-12] and only a few works studied the properties of PLD PSrT films prepared on Pt/SiO_2 substrate.[4-6] Therefore, this study investigates the influence of oxygen partial pressure on structural and electrical characteristics of PSrT films deposited by low-temperature PLD. Moreover, the relationship between the texture and the corresponding ferroelectricity of PLD-PSrT films is also addressed.

Experimental

p-Type silicon wafers with (100) orientation were employed as the substrate in this study. A 100 nm thick SiO_2 was grown after the initial RCA cleaning process. The platinum (Pt) film, 100 nm thick, was sputtered onto SiO_2/Si as the bottom electrode and followed by annealing at 450°C for 30 min in N_2 ambient.

Thin PSrT films (200 nm thick) were deposited on Pt/SiO_2/Si substrate electrodes with a KrF (λ = 248 nm) pulsed laser deposition system (Excimer Laser LPX 210i, Lambda Physik). A set of optical lenses was used to focus the excimer laser beam onto the ($Pb_{0.6}Sr_{0.4}$)TiO_3 target in vacuum. The PSrT target was prepared with a conventional ceramic fabrication process.[8] The vacuum chamber was pumped down to a base pressure of 0.1 mTorr and then refilled with O_2 as the working gas. The vaporized species of the target was transferred and deposited on the substrate heated by a thermal heater. The target-to-substrate distance was 4 cm. The deposition temperature was fixed at a relatively low substrate temperature of 400°C, calibrated at the wafer upper surface. The oxygen partial pressure (P_{O_2}) was varied from 50 to 200 mTorr. The laser pulsed rate and the average energy fluence were 5 Hz and 1.55 J/cm^2 per pulse, respectively.

The surface roughness of PSrT films was inspected by atomic force microscopy (AFM; DI Nano-Scope III, Digital Instruments Co.). Auger electron spectroscopy (AES; Auger 670 PHI Xi, Physical Electronics) was used to analyze the element depth profile. The crystallinity of the film was analyzed by X-ray diffractometer (D5000, Siemens Co., using Cu Kα, $\lambda \approx 0.154$ nm). Cross-sectional transmission electron microscopy (TEM) samples were prepared by standard sample preparation techniques with tripod polishing and ion milling using the Gatan PIPS system operated at 3 kV. The TEM experiments were carried out on a JEM-2000FX (JEOL, Ltd.) operated at 200 keV.

After the physical examination, the Pt top electrode, with a thickness of 100 nm and a diameter 75 μm, was deposited by sputtering and patterned by a shadow mask process to form a metal/ferroelectric/metal (MFM) capacitor structure. The noble metal platinum, with low resistivity, is considered as the electrode of

[z] E-mail: joewang666@gmail.com

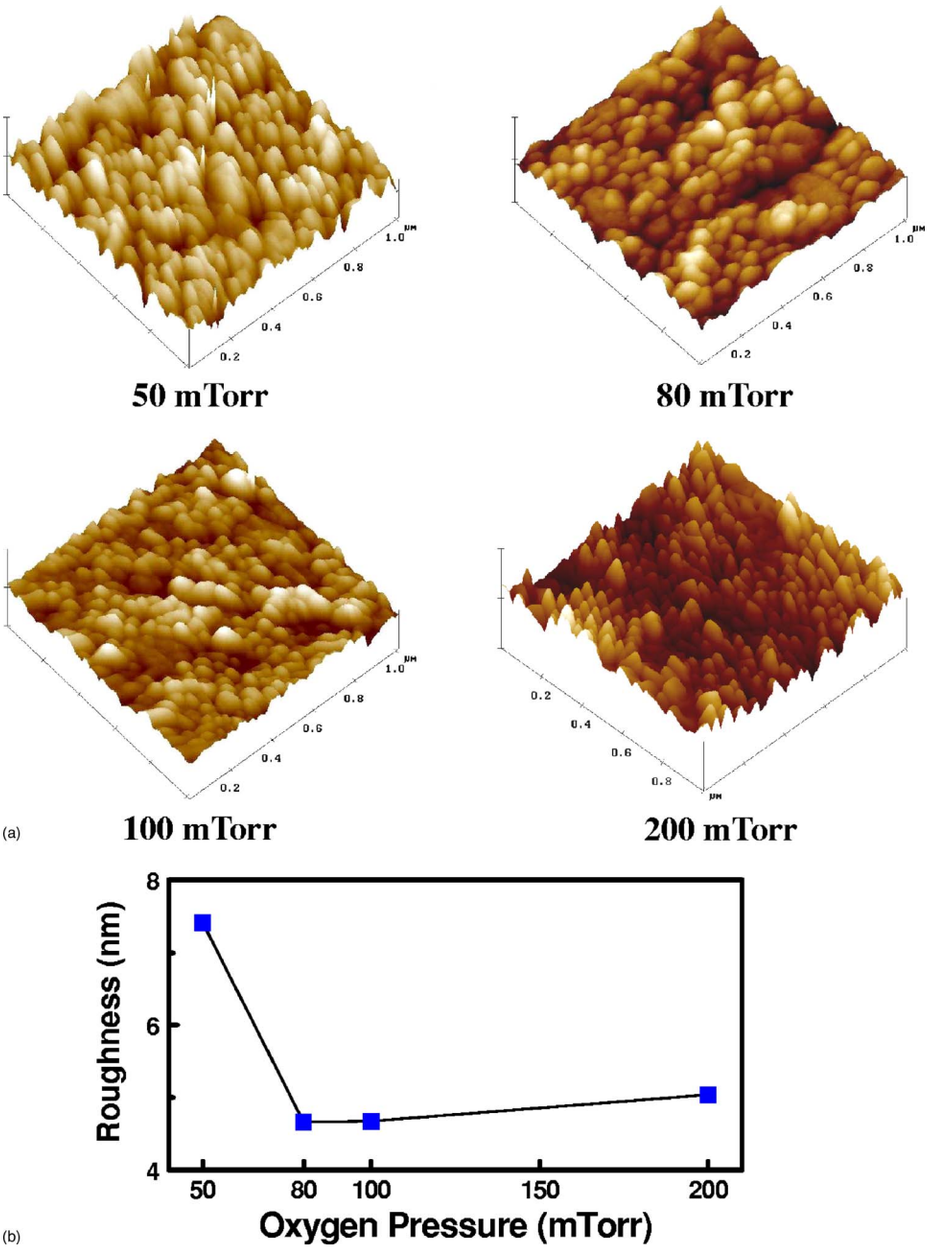

Figure 1. (Color online) (a) AFM images and (b) surface roughness of PLD PSrT films deposited at various oxygen partial pressures (P_{O_2}) on $Pt/SiO_2/Si(100)$ wafers.

Pt/PSrT/Pt capacitors because of its low power consumption and RC delay.[6] An automatic measurement system that combines an IBM PC/AT, semiconductor parameter analyzer (4156C, Agilent Technologies) and a probe station was used to measure the leakage current (*I-V* characteristics) and breakdown properties. A capacitance-voltage (*C-V*) analyzer (Package 82 system C-V 590, Keithley Co.) was also used to measure *C-V* curves at 100 kHz, and the dielectric constant was extracted from the *C-V* measurement.

Results and Discussion

Physical properties of PSrT films.— PLD PSrT films were prepared at various oxygen partial pressures (P_{O_2}). Figure 1a shows AFM images of PLD PSrT films deposited on $Pt/SiO_2/Si(100)$ wafers and indicates the surface morphology is a function of P_{O_2} associated with increasing collisions between ejected species and the ambient gas. For numerical analysis, Fig. 1b gives the normalized root-mean-square roughness (R_{rms}), revealing that the maximum R_{rms} and minimum R_{rms} are 7.41 and 4.66 nm as P_{O_2} equals 50 and 80 mTorr, respectively, and then R_{rms} increases very slightly as P_{O_2} increases. In short, films deposited at a higher P_{O_2} have smoother surface morphology. Figure 2 presents the intensity of the oxygen element in the AES depth profiles and indicates higher oxygen concentration for films deposited at higher P_{O_2}.

Figure 3a displays the X-ray diffraction (XRD) spectra of PSrT films deposited at various P_{O_2} on $Pt/SiO_2/Si(100)$ wafers. All of these spectra exhibit the diffraction peaks of $(Pb_{1-x}Sr_x)TiO_3$ perovskite phases.[1,2,6,13-16] The crystalline PSrT films are observed at such low temperature (400°C) because (*i*) the addition of strontium (Sr) induces a lower crystallization temperature of PSrT than that of PZT,[1] and (*ii*) the PLD technique can preserves the crystalline phases and stoichiometric ratio of the target material at low substrate temperature.[8] Furthermore, the intensity of the (100) and (110) diffraction peaks varies significantly as the oxygen partial pressure

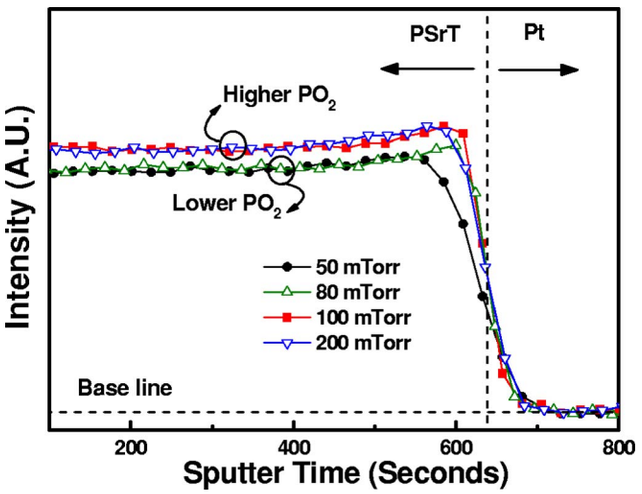

Figure 2. (Color online) Intensity of oxygen element in AES depth profiles of PSrT films deposited at various oxygen partial pressures on $Pt/SiO_2/Si(100)$ wafers.

increases. Figure 3b quantifies the XRD spectral analysis from the following formula,

$$X_{100} = I_{100}/(I_{100} + I_{110}) \quad [1]$$

where X_{100} is the relative proportion of the (100) orientation, I_{100} is the integrated area under the (100)-oriented peak, and I_{110} is the integrated area under the (110)-oriented peak. In Fig. 3b, I_{110} increases with increasing P_{O_2} and shows a maximum at P_{O_2} = 200 mTorr. In contrast, I_{100} exhibits the maximum at P_{O_2} = 80 mTorr and then decreases dramatically with increasing P_{O_2}. Thus, X_{100} shows the values as 51–55%, with a little variation at $P_{O_2} \leqslant 100$ mTorr, and then decreases noticeably as P_{O_2} increases from 100 to 200 mTorr. A transition from (100) preferred orientation to (110) preferred orientation of PSrT films is observed as P_{O_2} increases above 100 mTorr. According to the XRD result, it reveals the possibility exists to controlling the texture characteristics of PSrT films by oxygen partial pressure.

Figures 4a and b show cross-sectional TEM images of PSrT films deposited at 100 and 200 mTorr, respectively, revealing a column-like granular shape PSrT grain morphology. The corresponding selected-area diffraction patterns obtained from granular A and B (inserted in Fig. 4a and b) also reveal that the granular grains are single-crystal grains. Furthermore, the grain size of PSrT in the vertical (V) and horizontal (H) directions of columnar structures are strongly influenced by P_{O_2}. Figure 4c presents the grain size in the vertical and horizontal directions of granular PSrT grains from the TEM images. The grain size in vertical direction increases with increasing P_{O_2}, and the maximum grain size is close to film thickness (200 nm) as P_{O_2} = 200 mTorr. In contrast, the horizontal grain size shrinks as P_{O_2} increases and reaches the minimum at 200 mTorr. As mentioned above, it is clear that the surface morphology, surface roughness, oxygen composition, preferred orientation, and microstructure of PSrT films could apparently be affected by oxygen partial pressures during PLD.

Electrical characteristics of PSrT films.— Figure 5a plots the capacitance vs electric field (*C-E*) characteristics of the PSrT films deposited at various P_{O_2} and presents the typical *C-E* hysteresis characteristics of ferroelectric materials. The capacitance shows a maximum value at negative bias corresponding to the coercive field (E_c) of the hystersis loop as the applied field sweeps from +200 to −200 kV/cm. The maximum capacitance appears at positive E_c when the applied field sweeps in the opposite direction. The

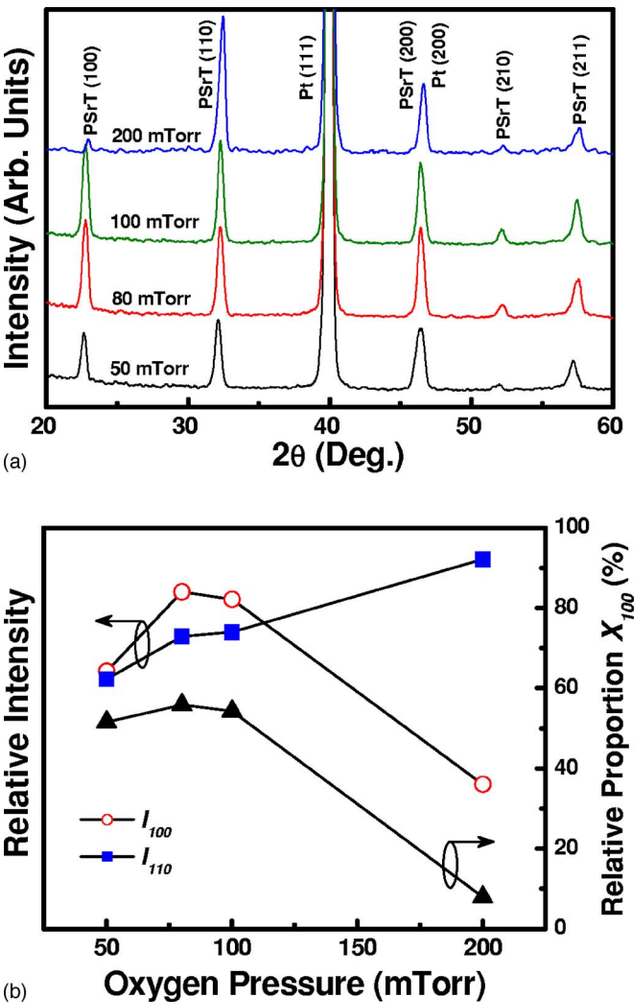

Figure 3. (Color online) X-ray diffraction analyses of PSrT films deposited at various oxygen partial pressures on $Pt/SiO_2/Si(100)$ wafers: (a) diffraction spectra and (b) texture characteristics.

four *C-E* curves are not symmetric, probably because of the difference in the configuration of electrodes used in the measurement, because the bottom electrode has a large area and the other, defined by a shadow mask, is small. Furthermore, the *C-E* hysteresis loop expands from P_{O_2} = 50 mTorr to 100 mTorr and then shrinks as P_{O_2} is higher than 100 mTorr, suggesting that the ferroelectricity of PSrT films is suppressed at higher P_{O_2} (200 mTorr). The ferroelectricity of ferroelectric material could be obtained analytically by calculating the polarization P from the relative permittivity (ε_r) vs electric field (E) using the following formula

$$P = \varepsilon_0 \times \int (\varepsilon_r - 1) dE \quad [2]$$

where ε_0 is the vacuum permittivity and ε_r is obtained from *C-V* relations. The zero-field capacitance, used in the dielectric constant calculation as shown in Fig. 5b, depends considerably on the P_{O_2}. The polarization of the lead-titanate-based crystal is maximum in the [100] direction, so the polarizations of the films enhanced with the preferred (110) orientation are weaker than those of the films with the preferred (100) orientation.[17,18] Furthermore, the tetragonality (c/a), i.e., the ratio of c axis/a axis lattice constant obtained by electron diffraction patterns (not shown in this work) of the PSrT films deposited at 50 mTorr and 200 mTorr are ~1.033 and ~1,

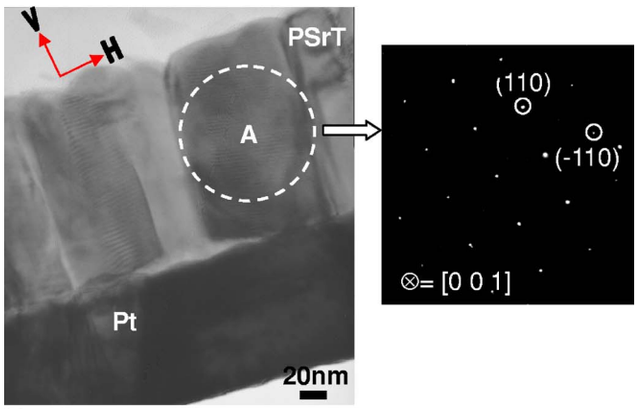

(a)

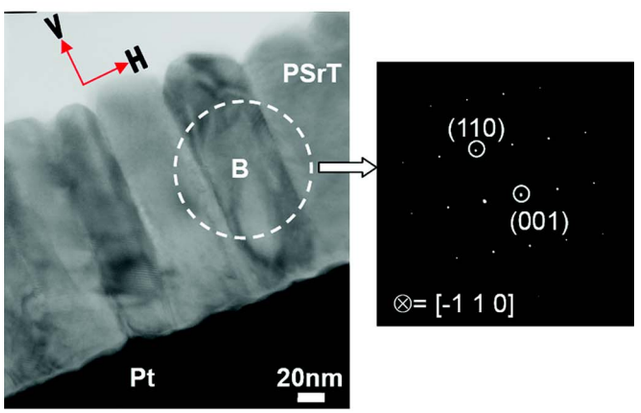

(b)

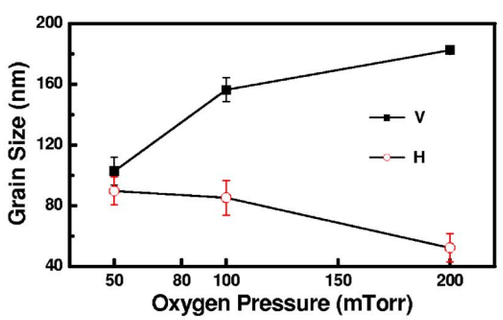

(c)

Figure 4. (Color online) Cross-sectional TEM images and selected-area diffraction patterns of PLD PSrT films deposited at (a) P_{O_2} = 100 mTorr and (b) P_{O_2} = 200 mTorr. (c) Grain size in the vertical (V) and horizontal (H) directions of columnar structures.

accordingly. The larger tetragonality for films deposited at lower P_{O_2} may be attributed to the oxygen deficiency.[19-21] Because the ferroelectric dipole originates from ionic displacement in the *c*-axis direction, large spontaneous polarization is obtained with the elongated *c* axis, the larger tetragonality. However, the lower P_{O_2}-deposited film (the most oxygen deficient) exhibits larger leakage current density (addressed later), which usually degrades the dielectric constant. In other words, the dielectric and ferroelectric properties of PSrT films are the combined effects of the preferred-orientation and oxygen content. Thus, the PSrT film deposited at 100 mTorr exhibits the maximum dielectric constant of 642, which is connected with the enhanced (100) preferred orientation (Fig. 3b) and the higher oxygen concentration (Fig. 2).

Figure 6 shows that the time-zero dielectric breakdown (TZDB)

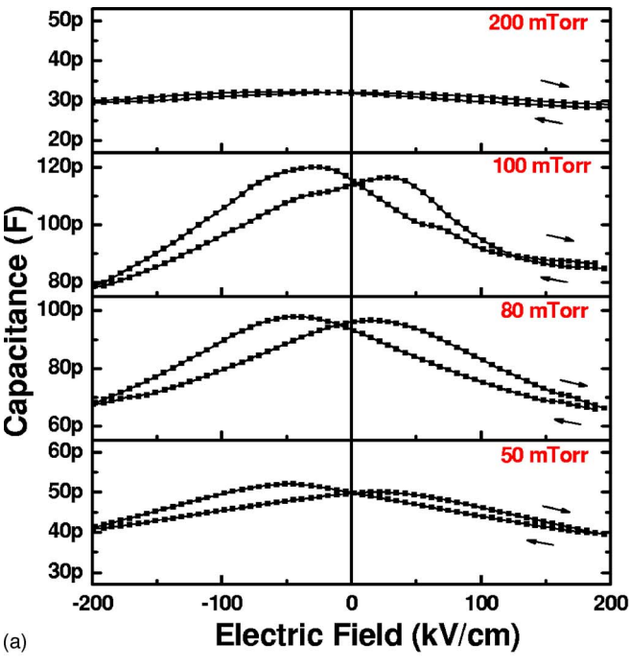

(a)

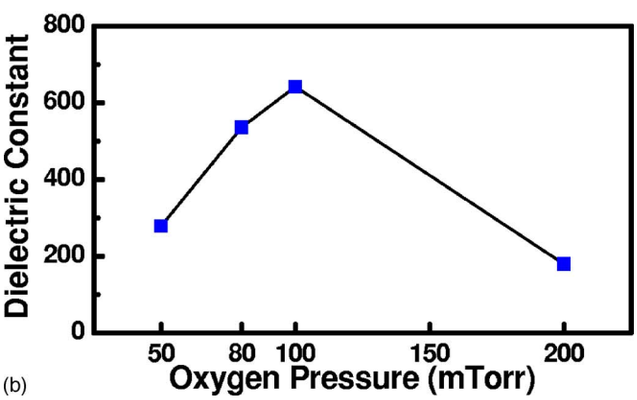

(b)

Figure 5. (Color online) (a) Capacitance vs electric field (*C-E*) hysteresis loops and (b) dielectric constant of Pt/PSrT/Pt capacitors prepared at various oxygen partial pressures.

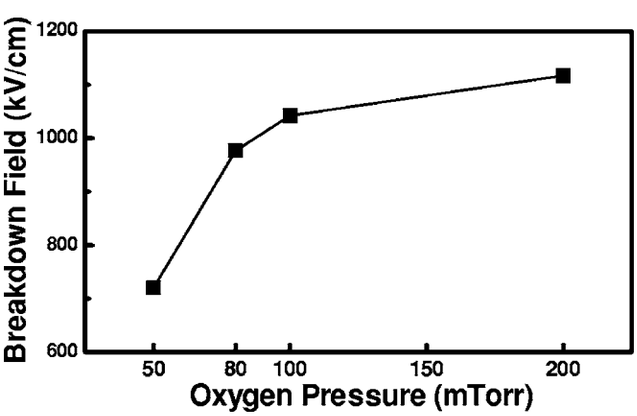

Figure 6. TZDB of PSrT films deposited at various oxygen partial pressures.

Table I. Summarized characteristics of PLD PSrT films deposited at various oxygen partial pressures on Pt/SiO_2/Si(100) wafers.

Oxygen partial pressure (P_{O_2}, mTorr)	50	80	100	200
RMS roughness (R_{RMS}, nm)[a]	7.41	4.66	4.68	5.04
X_{100} Relative proportion (%)[b]	51.5	55.8	54.3	7.9
TZDB field (kV/cm)	721	976	1042	1117
Dielectric constant[c]	279	536	642	180
Current density ($\mu A/cm^2$)[d]	0.812	0.416	0.187	0.119

[a] Evaluated from AFM analysis.
[b] Evaluated from XRD spectra.
[c] Evaluated from *C-E* curves at zero field.
[d] Evaluated from *J-E* curves at +100 kV/cm.

of the Pt/PSrT/Pt capacitor is enhanced as P_{O_2} increases. TZDB is influenced by grain size and oxygen stoichiometry of the films because of a large potential drop across the high-resistivity grain boundary, and because the space charge of oxygen vacancies (OVs) causes resistance degradation as expressed by the following reaction[22-24]

$$O_o \leftrightarrow V_o^{\cdot\cdot} + 2e' + \frac{1}{2} O_2, \quad [3]$$

where O_o, $V_o^{\cdot\cdot}$, and e' represent the oxygen ion on its normal site, the oxygen vacancy, and the electron, respectively. The PSrT films deposited at higher P_{O_2} exhibit a higher breakdown field, due presumably to the fewer OVs (i.e., higher oxygen concentration shown in Fig. 2).

Table I summarizes the physical properties and electrical characteristics of PLD PSrT films deposited at various oxygen partial pressures on Pt/SiO_2/Si(100) wafers. It can be seen that the leakage current density biased at +100 kV/cm decreases as P_{O_2} increases. Later in the text, the leakage current data are interpreted as Schottky emission (SE) at lower electric fields and Poole–Frenkel emission (PF) at higher electric fields, which are used to analyze the interface-limited and bulk-limited characteristics of Pt/PSrT/Pt capacitors, respectively.[24-26] The SE behavior is expressed as

$$\text{SE:}\log(J_{SE}/T^2) = -q[\varphi_B - (qE/4\pi\varepsilon_d\varepsilon_0)^{1/2}]/(kT\ln 10) + \log(A^*) \quad [4]$$

where A^* is the effective Richardson's constant, φ_B is the potential barrier height at the interface, ε_d is the dynamic dielectric constant of the ferroelectric material in the infrared region, q is the unit charge, k is Boltzmann's constant, J is current density, T is absolute temperature, and E is the external electric field. If the conduction current follows SE behavior, then a $\log(J/T^2)$ vs $E^{1/2}$ plot should be linear. Similarly, a $\log(J/E)$ vs $E^{1/2}$ plot can be made for PF. Figure 7a presents the SE plot of Pt/PSrT/Pt capacitors deposited at various P_{O_2} and the dashed lines represent the fitted results. The inhibited leakage current of PSrT films deposited at higher P_{O_2} is correlated with the lower Schottky barrier, fewer interface states and fewer space charges (charged OVs) due to the smoother surface morphology (Fig. 1) and fewer OVs. The result is consistent with the breakdown field of TZDB (Fig. 6). As seen in Fig. 7a, this indicates that films deposited at 200 mTorr exhibit SE conduction only (without a transition of conduction). Figures 7b and c draw the electron energy band at the interface of substrate electrodes and reveals PSrT films act as n-type semiconductors due to the generation of OVs in ABO_3 perovskites.[24,27] In the case with lower P_{O_2}, more interface states result in more charge accumulation and severe image-force effects at

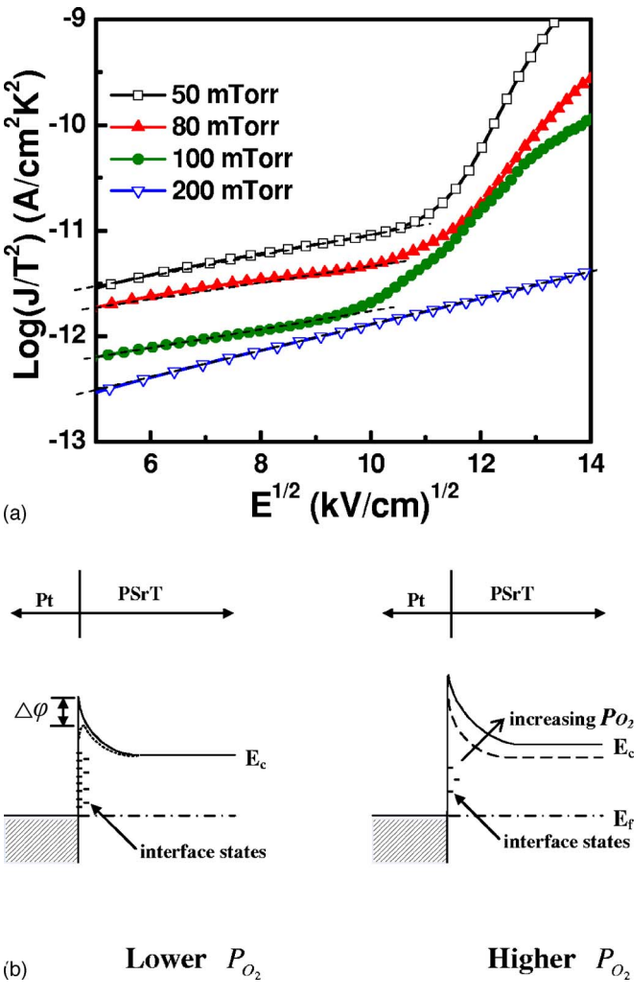

Figure 7. (Color online) (a) Experimental and fitted log (J/T^2) vs $E^{1/2}$ (Schottky emission) plots, and the electron energy band at the interface of substrate electrodes for PSrT films deposited at (b) lower P_{O_2} and (c) higher P_{O_2}.

the edge of the electrodes, leading to the decrease ($\Delta\varphi$) of Schottky barrier height.[27,28] In the case with higher P_{O_2}, the increase of P_{O_2} yields fewer interface states and a higher Schottky barrier, resulting in a small leakage current.

Figure 8a shows the PF plot using the same experimental *I-V* data, given by the following equation, indicating that the curves follow PF behavior when the bias exceeds +130 kV/cm and trapping states exist for PLD-PSrT films deposited at 50–100 mTorr.

$$\text{PF:}\log(J_{PF}/E) = -q[\varphi_t - (qE/\pi\varepsilon_d\varepsilon_0)^{1/2}]/(kT\ln 10) + \log(B) \quad [5]$$

where B is a constant, and φ_t is the trapped energy level. In contrast, the leakage current of PSrT films deposited at P_{O_2} = 200 mTorr is not governed by PF. Figure 8b reveals that PSrT films deposited at lower P_{O_2} have more OVs and rougher surface than those deposited at higher P_{O_2}, yielding more interfacial states as stated in Fig. 7b and more trapping states inside PSrT films. Thus, the magnitude of leakage current is governed by the balance between the injected electron current and the trapping/detrapping rate. The field-assisted emission of trapped charged carriers follows PF emission rate, revealing bulk-limited conduction as the dominant mechanism for the lower P_{O_2} case. In contrast, Fig. 8c indicates that higher P_{O_2} yields fewer interfacial states with the higher barrier and fewer trapping

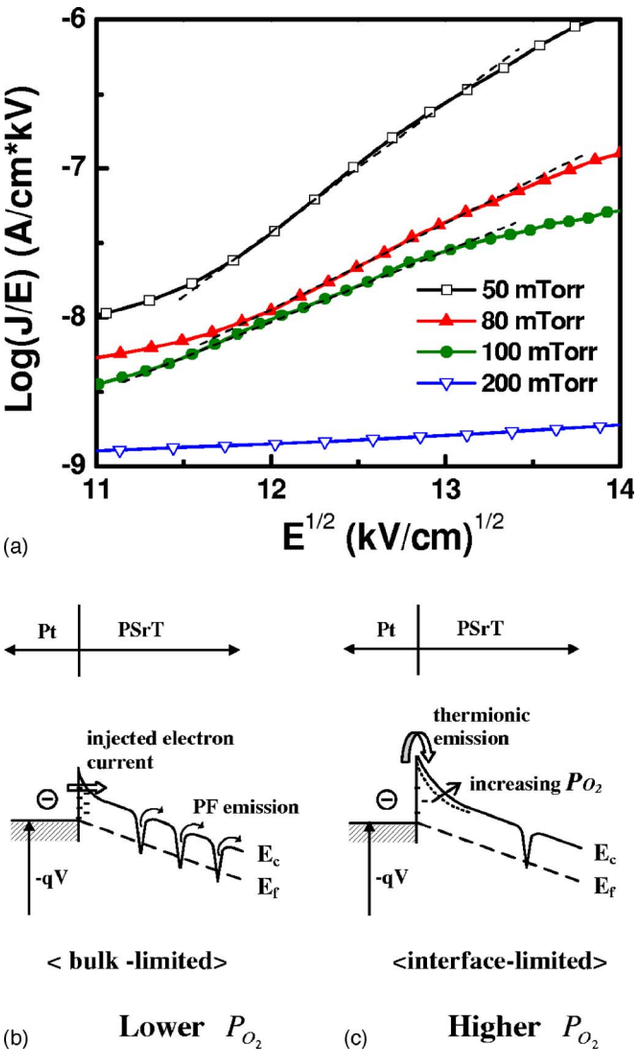

Figure 8. (Color online) (a) Experimental and fitted log (J/E) vs $E^{1/2}$ (Poole–Frenkel emission) plot, and the electron energy band for PSrT films deposited at (b) lower P_{O_2} and (c) higher P_{O_2}.

states inside PSrT films, caused by a smoother surface and fewer OVs. Therefore, thermionic emission (SE behavior), i.e., interface-limited conduction, is the dominant mechanism at higher P_{O_2}. Consequently, except for the PSrT films deposited at 200 mTorr which reveal SE behavior at the applied field range, the conduction mechanism of PLD PSrT films reveals interface-limited (SE) conduction at low electric field and changes to bulk-limited (PF) conduction at high electric field.

Conclusions

The preferred orientation, microstructure, and electrical characteristics of PSrT films apparently could be apparently affected by oxygen partial pressures during low-temperature PLD. The smoother surface morphology, the higher oxygen composition, and the stronger intensity of (110) orientation could be evidently influenced by increasing P_{O_2} during PLD. In addition, the (100) preferred orientation transits to (110) preferred orientation above 100 mTorr, suggesting that the ferroelectricity of PSrT films is suppressed at higher P_{O_2}. The paraelectricity/ferroelectricity transition and dielectric constant are associated with the preferred orientation and oxygen concentration. Moreover, the PSrT films deposited at higher P_{O_2} exhibit a higher breakdown field due presumably to the fewer oxygen vacancies (OVs). It is also seen that the leakage current density biased at +100 kV/cm decreases as a function of P_{O_2}. The leakage current analysis of Pt/PSrT/Pt capacitors reveals SE/PF (Schottky emission/Poole–Frenkel emission) at low/high applied field, except the PSrT films deposited at P_{O_2} = 200 mTorr only reveal SE behavior at the applied field range. The increased P_{O_2} yields fewer interface states and a higher Schottky barrier and fewer trapping states inside PSrT films. Furthermore, the conduction mechanism of PLD PSrT films changes from bulk-limited (PF) to interface-limited (SE) as P_{O_2} increases. PLD PSrT films, deposited at oxygen partial pressures from 50 to 200 mTorr, have been demonstrated with dense surface morphologies, good crystallinity, single-crystal grains in column-like granular structure, and excellent electrical properties. Hence, the PLD PSrT film is a promising material for integration in integrated-circuit-compatible process.

Acknowledgments

This work was supported in part by the National Science Council of the Republic of China under contract no. NSC95-2221-E-009-253. Thanks are also due to the Nano Facility Center (NFC) in National Chiao Tung University, the Center for Condensed Matter Sciences in National Taiwan University and the National Nano Device Laboratory (NDL) of the NSC for the technical supports.

National Chiao Tung University assisted in meeting the publication costs of this article.

References

1. D. H. Kang, J. H. Kim, J. H. Park, and K. H. Yoon, *Mater. Res. Bull.*, **36**, 265 (2001).
2. F. Zhang, T. Karaki, and M. Adachi, *Jpn. J. Appl. Phys., Part 1*, **44**, 6995 (2005).
3. T. Karaki, J. Du, T. Fujii, and M. Adachi, *Jpn. J. Appl. Phys., Part 1*, **41**, 6761 (2002).
4. C. C. Chou, C. S. Hou, G. C. Chang, and H. F. Cheng, *Appl. Surf. Sci.*, **142**, 413 (1999).
5. C. C. Chou, C. S. Hou, and H. F. Cheng, *Ferroelectrics*, **206–207**, 393 (1998).
6. C. S. Hou, H. C. Pan, C. C. Chou, and H. F. Cheng, *Ferroelectrics*, **232**, 129 (1999).
7. D. G. Lim, Y. Park, S. I. Moon, and J. Yi, *Applications of Ferroelectrics 2000, ISAF 2000, Proceedings of the 2000 12th IEEE International Symposium*, Honolulu, HI, p. 599 (2000).
8. D. B. Chrisey and G. K. Huber, *Pulsed Laser Deposition of Thin Films*, pp. 55–87 and pp. 167–198, Wiley-Interscience Publications, New York (1992).
9. A. R. James and C. Prakash, *Appl. Phys. Lett.*, **84**, 1165 (2004).
10. N. Scarisoreanu, F. Craciun, G. Dinescu, P. Verardi, and M. Dinescu, *Thin Solid Films*, **453–454**, 399 (2004).
11. R. C. Rodrigueza, S. P. Sanchez, B. E. Watts, and F. Leccabue, *Mater. Lett.*, **57**, 3958 (2003).
12. X. S. Gao, J. M. Xue, J. Li, C. K. Ong, and J. Wang, *Microelectron. Eng.*, **66**, 926 (2003).
13. C. C. Chou, H. Y. Chang, I. N. Lin, B. J. Shaw, and J. T. Tan, *Jpn. J. Appl. Phys., Part 1*, **37**, 5269 (1998).
14. H. C. Pan, G. C. Chang, C. C. Chou, and H. F. Cheng, *Integr. Ferroelectr.*, **25**, 179 (1999).
15. H. J. Chung, J. H. Kim, and S. I. Woo, *Chem. Mater.*, **13**, 1441 (2001).
16. H. J. Chung and S. I. Woo, *J. Vac. Sci. Technol. B*, **19**, 275 (2001).
17. H. N. Al-Shareef and A. I. Kingon, in *Ferroelectric Thin Films: Synthesis and Basic Properties, Ferroelectric and Related Phenomena*, Vol. 10, C. P. De Araujo, J. F. Scott, and G. W. Taylor, Editors, pp. 193–226 and pp. 447–478, Gordon and Breach Publishers, The Netherlands (1996).
18. Y. Xu, *Ferroelectric Materials and Their Applications*, pp. 101–162, Elsevier Science Publishers, B.V., Amsterdam (1991).
19. C. L. Li, Z. H. Chen, Y. L. Zhou, and D. F. Cui, *J. Phys. Condens. Matter*, **13**, 5361 (2001).
20. D. Fuchs, M. Adam, P. Schweiss, S. Gerhold, S. Schuppler, R. Schneider, and B. Obst, *J. Appl. Phys.*, **88**, 1844 (2000).
21. D. F. Cui, H. S. Wang, Z. H. Chen, Y. L. Zhou, H. B. Lu, and G. Z. Yang, *J. Vac. Sci. Technol. A*, **15**, 275 (1997).
22. R. Waster, R. T. Baiatu, and K. H. Haratl, *J. Am. Ceram. Soc.*, **73**, 1645 (1990).
23. M. S. Tsai and T. Y. Tseng, *IEEE Trans. Compon. Packag. Technol.*, **23**, 128 (2000).
24. D. C. Shye, B. S. Chiou, M. J. Lai, C. C. Hwang, C. C. Jiang, J. S. Chen, M. H. Cheng, and H. C. Cheng, *J. Electrochem. Soc.*, **150**, F20 (2003).
25. A. Vorobiev, P. Rundqvist, K. Khamchahe, and S. Gevorgian, *J. Appl. Phys.*, **96**, 4642 (2004).
26. S. Ezhivalavan, V. Samper, T. W. Seng, X. Junmin, and J. Wang, *J. Appl. Phys.*, **96**, 2181 (2004).
27. J. F. Scott, *Ferroelectric Memories*, pp. 79–85, Springer-Verlag, Berlin (2000).
28. J. Burm and L. F. Eastman, *IEEE Photonics Technol. Lett.*, **8**, 113 (1996).